ARTICLES
https://doi.org/10.1038/s41558-021-01077-8
nature climate change

Check for updates

Rapid increases and extreme months in projections of United States high-tide flooding

Philip R. Thompson[1,2]✉, Matthew J. Widlansky[2], Benjamin D. Hamlington[3], Mark A. Merrifield[4], John J. Marra[5], Gary T. Mitchum[6] and William Sweet[7]

Coastal locations around the United States, particularly along the Atlantic coast, are experiencing recurrent flooding at high tide. Continued sea-level rise (SLR) will exacerbate the issue where present, and many more locations will begin to experience recurrent high-tide flooding (HTF) in the coming decades. Here we use established SLR scenarios and flooding thresholds to demonstrate how the combined effects of SLR and nodal cycle modulations of tidal amplitude lead to acute inflections in projections of future HTF. The mid-2030s, in particular, may see the onset of rapid increases in the frequency of HTF in multiple US coastal regions. We also show how annual cycles and sea-level anomalies lead to extreme seasons or months during which many days of HTF cluster together. Clustering can lead to critical frequencies of HTF occurring during monthly or seasonal periods one to two decades prior to being expected on an annual basis.

The impact of high-tide flooding (HTF) accumulates over numerous seemingly minor occurrences, which can exceed the impact of rare extremes over time[1–3]. These impacts are subtle—for example, the loss of revenue due to recurrent road and business closures[4]—compared with the physical damage of property and infrastructure associated with extreme storm-driven events. As sea-level rise (SLR) increases the frequency of HTF in the United States[5–11], coastal communities will need to adapt. However, developing adaptation pathways for recurrent coastal flooding is challenging and requires knowledge of environmental and social tipping points at which current actions and policies become ineffective[12–14].

Here we characterize projected increases in US HTF (including the impact of the 18.6-year nodal cycle in tidal amplitude[15–17]) in a way that can be used to establish planning horizons and develop adaptation pathways. First, we focus on the rate of flooding-frequency increase, which is not well understood despite being critical to establishing SLR impact timelines[18]. More specifically, we examine acute inflections, or tipping points, in the rate of increase that mark transitions from periods of gradual (and potentially imperceptible) change to rapid increase in HTF frequency. Second, we focus on the tendency of HTF episodes to cluster in time[19]. Scientists, engineers and decision-makers are accustomed to the statistics and impacts of isolated extreme events[20–23], but given the cumulative nature of HTF impacts[1–3], we describe extreme months or seasons during which the number of flooding episodes, rather than the magnitude, is exceptional.

Projections of HTF frequency

Ensemble projections of twenty-first-century HTF frequency (Methods) are generated for 89 tide-gauge locations across the contiguous United States and US-affiliated Pacific and Caribbean islands (Supplementary Data). HTF frequencies are represented as counts of days in monthly and annual windows for which at least one hourly sea-level value exceeds the flooding threshold of interest. US National Oceanic and Atmospheric Administration (NOAA) SLR scenarios[24] and derived HTF thresholds[10], which are ubiquitous in US coastal planning, are used to produce the projections. NOAA minor and moderate flooding thresholds correspond to levels 50–60 cm and 80–90 cm, respectively, above the local mean higher high water tidal datum[10] (Supplementary Data). Here we focus on the NOAA Intermediate Low and Intermediate SLR scenarios corresponding to 0.5 m and 1.0 m, respectively, of global mean SLR by 2100. At present, it is not possible to assess which of the NOAA SLR scenarios the observations are tracking due to decadal variability in global and local sea level[25–27] and the lack of divergence in the scenarios (<2 cm) during 2000–2020. However, these two scenarios bracket the bulk of global and local SLR possibilities during the twenty-first century, being roughly equivalent to the 4th and 83rd percentiles[24] of probabilistic local sea-level projections[28] based on IPCC Fifth Assessment Report Representative Concentration Pathway 8.5 (ref. [29]).

Under the Intermediate scenario, annual projections of HTF days from different regions of the US coastline show dramatic increases in HTF frequency over the next 30–40 years (Fig. 1). The 10th–90th percentile range of each ensemble projection represents the degree to which the count in any given year can vary due to local sea-level variability across a variety of processes and timescales from high-frequency surge to decadal climate variability. Including the effect of local sea-level variability is essential for producing useful HTF projections, as SLR and astronomical tides alone will underestimate HTF frequency (Extended Data Fig. 1)[10]. Note that the range of projections over the ensemble at each location should not be interpreted as a true uncertainty, because uncertainty in anthropogenic SLR is excluded in this case by using a discrete NOAA SLR scenario. Incorporating uncertainty in SLR (as in the probabilistic projection[28] from which the NOAA scenarios are extracted[24]) would produce a much wider range of possibilities.

Rapid transitions in the frequency of HTF

The projections in Fig. 1 exhibit an important commonality: pronounced inflections in HTF frequency before mid-century. Such

[1]Department of Oceanography, University of Hawai'i at Mānoa, Honolulu, HI, USA. [2]Joint Institute for Marine and Atmospheric Research, University of Hawai'i at Mānoa, Honolulu, HI, USA. [3]NASA Jet Propulsion Laboratory, Pasadena, CA, USA. [4]Scripps Institution of Oceanography, University of California, San Diego, La Jolla, CA, USA. [5]Inouye Regional Center, NOAA/NESDIS/National Centers for Environmental Information, Honolulu, HI, USA. [6]College of Marine Science, University of South Florida, St. Petersburg, FL, USA. [7]NOAA/National Ocean Service, Silver Spring, MD, USA. ✉e-mail: philiprt@hawaii.edu

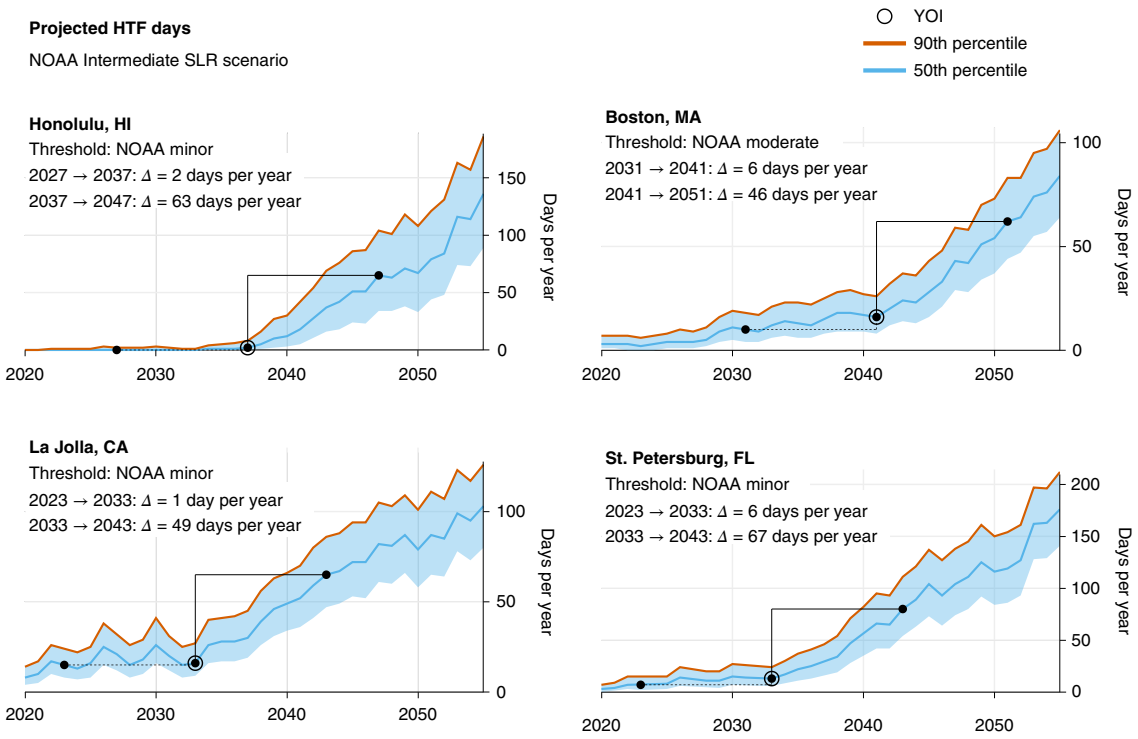

Fig. 1 | Projections of annual counts of HTF days for the NOAA Intermediate SLR scenario. The NOAA minor flooding threshold is used for Honolulu, San Diego and St. Petersburg. The NOAA moderate flooding threshold is used for Boston to highlight a threshold that is not yet routinely exceeded, which is not the case for the Boston minor threshold[11]. The 50th percentile from the ensemble of projections (blue line) and the 10th–90th percentile range (blue shading, with the 90th percentile highlighted in orange) show increasing numbers of HTF days per year. The YOI (open black circle) for each projection corresponds to abrupt increases in the frequency of HTF days, which are highlighted by comparing the projected increases (Δ) over two adjacent ten-year periods (dashed and solid black lines).

inflections, or tipping points, are essential for planning, because they represent transitions from regimes of gradual—and in some cases almost imperceptible—change to regimes of rapid increase in HTF frequency. These transitions can produce acute impacts in unsuspecting and underprepared communities if not identified in advance and communicated to stakeholders and decision-makers. The timing and severity of inflections are related to multiple factors. First, present-day HTF in most locations occurs during only the highest astronomical tides of the year. With SLR, increasing moderate (and more common) high tides will reach flood thresholds, resulting in a rapid increase in the number of HTF days. Second, high-tide amplitudes vary predictably in space and time due to astronomical forcing over timescales from monthly (that is, spring–neap cycles) to decadal (that is, the 18.6-year nodal cycle; see below). The interplay between SLR elevating increasing numbers of high tides towards the threshold and modulations of the tidal amplitude by astronomical forces dictates the timing and nature of inflections in HTF frequency.

To investigate contributions to projected rapid HTF increases, we identify a year of inflection (YOI) for each combination of tide-gauge location, scenario and threshold (Methods). In practice, a continuum of YOIs exists at each location corresponding to the range of possibilities for threshold height and evolution of twenty-first-century SLR. While the YOIs here are specific to the scenarios and thresholds used, they indicate the approximate timing at which rapid transitions will occur for similar scenarios and thresholds. For the four highlighted cases (Fig. 1), the YOI marks the end of a decade experiencing little increase in the expected number of HTF days per year, while decades following the YOIs experience a quadrupling or more.

YOI timing at the four locations is linked to modulations of tidal amplitude associated with the 18.6-year nodal cycle[15,16]. For example, in St. Petersburg, the nodal cycle range is 4.7 cm, representing the peak-to-trough difference in the height of the highest (annual 99th percentile) astronomical tides over a nodal cycle (Fig. 2, left). While not large compared with nodal cycle ranges exceeding 20 cm in other parts of the world[30], the range in St. Petersburg is sufficient to impact the evolution of increasing HTF. During 2024–2033, the Intermediate scenario projects 8.9 cm of SLR in St. Petersburg (Fig. 2, left). The height of the highest tides, however, is projected to increase by just 4.3 cm due to decreasing tidal amplitude associated with the nodal cycle. The opposite occurs during the following decade, and the increase in the height of the highest tides (14.1 cm) is enhanced relative to SLR (9.4 cm). Importantly, the decadal difference in high-tide height increase in St. Petersburg (14.1 − 4.3 = 9.8 cm) is larger than a decade of projected SLR (~9 cm per decade for the Intermediate scenario).

In St. Petersburg, the ratio of the nodal cycle range to a decade of projected SLR is roughly 0.5. Calculating this ratio across the United States highlights locations and regions where the nodal cycle is of sufficient magnitude to contribute to rapid inflections in HTF frequency (Fig. 2, right). Ratios in many locations, including 73% along the Pacific and Gulf of Mexico coastlines, exceed 0.4. In the near term, such locations are most susceptible to rapid inflections in HTF frequency due to the confluence of SLR and nodal cycle modulations of tidal amplitude.

The projection algorithm employed here (Methods) explicitly incorporates twenty-first-century predictions of astronomical tides and captures the effects of long-period tidal modulation on HTF frequency. The nonlinear relationship between the height of the

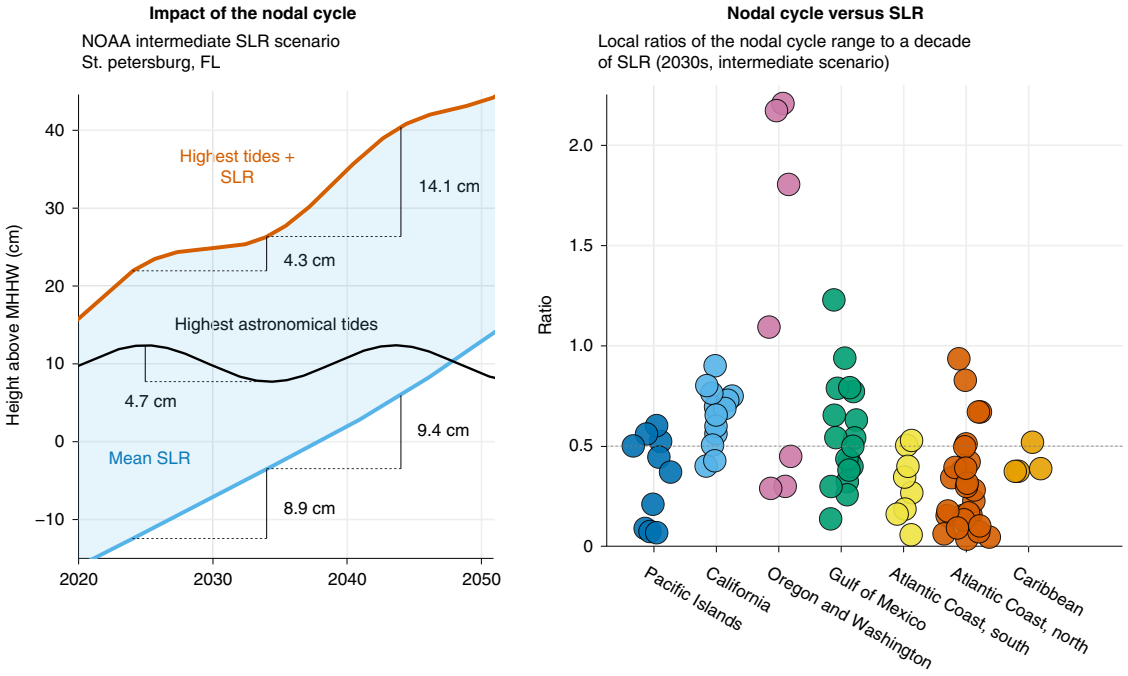

Fig. 2 | Impact of the nodal cycle. Left, projected heights of the highest tides in St. Petersburg, Florida (red), due to the combination of projected mean SLR (blue, NOAA Intermediate SLR scenario) and the 18.6-year nodal cycle expressed in the annual 99th percentile of astronomical tidal height (black). All time series are relative to the current mean higher high water (MHHW) tidal datum. Right, ratios at each US tide-gauge location of nodal cycle peak-to-trough range to ten years of projected SLR (2030s, NOAA Intermediate SLR scenario). The dot colours correspond to US coastal regions.

highest tides and HTF frequency (Methods) further amplifies the inflection in the HTF projection, which manifests in a rapid increase from 13 to 80 HTF days per year on average in St. Petersburg over the decade following the YOI in 2033 (Fig. 1, lower right). Not coincidentally, the YOI for St. Petersburg also corresponds to the nodal cycle minimum in tidal amplitude, marking the transition between suppression and enhancement of increasing high-tide height by the nodal cycle.

YOI timing around the United States tends to be similar (though not uniform) within regions (Fig. 3 and Supplementary Data). Timing generally depends on (1) threshold height, (2) local rates of relative SLR and (3) the timing of nodal cycle minima in tidal amplitude. Higher rates of relative SLR and/or lower thresholds lead to earlier YOIs. Glacial isostatic adjustment[31] can offset absolute SLR, leading to YOIs later in the century (for example, in Oregon and Washington). The relative importance of the nodal cycle varies with the ratios in Fig. 2. For locations and regions where the nodal cycle is a leading order contribution to changes in HTF, YOIs tend to occur near minima in tidal amplitude. We note, however, that the timing of minima in tidal amplitude varies regionally depending on the tidal constituent for which nodal cycle modulations are most prominent. For Hawai'i, the Pacific Coast and the Gulf of Mexico, the nodal cycle is most prominent in modulations of the lunar diurnal (K1) tidal constituent, which has amplitude minima in the mid-2030s, mid-2050s and early 2070s. For northern portions of the Atlantic coast, the nodal cycle is most prominent in modulations of the lunar semidiurnal (M2) tidal constituent, which has amplitude minima in the mid-2020s, mid-2040s and early 2060s. Hence, the YOI for Boston in Fig. 1 occurs in the mid-2040s, while YOIs for the other three cases occur in the mid-2030s.

The purpose of the YOI calculation is to provide a marker for the potential onset of rapid HTF increases. The severity of the increase following YOIs is indicated in two ways in Fig. 3. The values along the vertical axis correspond to absolute increases in the expected number of HTF days per year during the decade following each YOI. The sizes of the markers correspond to relative increases (that is, ten-year multipliers) in HTF days per year over the decade following the YOI. The most acute inflections occur where the ten-year period following the YOI experiences both large absolute (that is, the upper portion of the vertical-axis domain) and large relative (that is, large marker) changes.

Under the Intermediate scenario, many Atlantic locations will experience modest inflections in the frequency of minor HTF in the mid-2020s (Fig. 3, top), which in some cases correspond to minima in nodal cycle modulations of the M2 tidal constituent. The relative ten-year increases for Atlantic locations are generally modest compared with those for other regions, because the minor threshold is already routinely exceeded for many of these sites[11]. Around the mid-2030s, locations along the Pacific and Gulf of Mexico coastlines will experience rapid increases in HTF frequency (Fig. 3, top). The timing and severity of inflections in these regions are influenced by nodal cycle modulations of the K1 tidal constituent and are generally associated with large ten-year multipliers, indicating transitions from few to many HTF days per year. Under the Intermediate SLR scenario, 71% of Pacific Island, California and Gulf of Mexico locations will experience at least a tripling, and 59% at least a quadrupling, of minor HTF days per year over a ten-year period beginning in the 2030s.

NOAA moderate flooding thresholds are rarely exceeded at present[11]. For the Intermediate SLR scenario, rapid transitions in moderate HTF tend to begin in the mid-2040s along the Atlantic coast and during the 2050s for the Pacific and Gulf coasts (Fig. 3, bottom). Exceptions include Gulf of Mexico locations (for example, Grand Isle, Louisiana, and Galveston, Texas) where YOIs occur during the mid-2030s due to high subsidence rates and substantially larger relative SLR. In general, YOIs for moderate thresholds occur later in the century than those for minor thresholds. Since the projected rate of SLR accelerates during the twenty-first century, YOIs

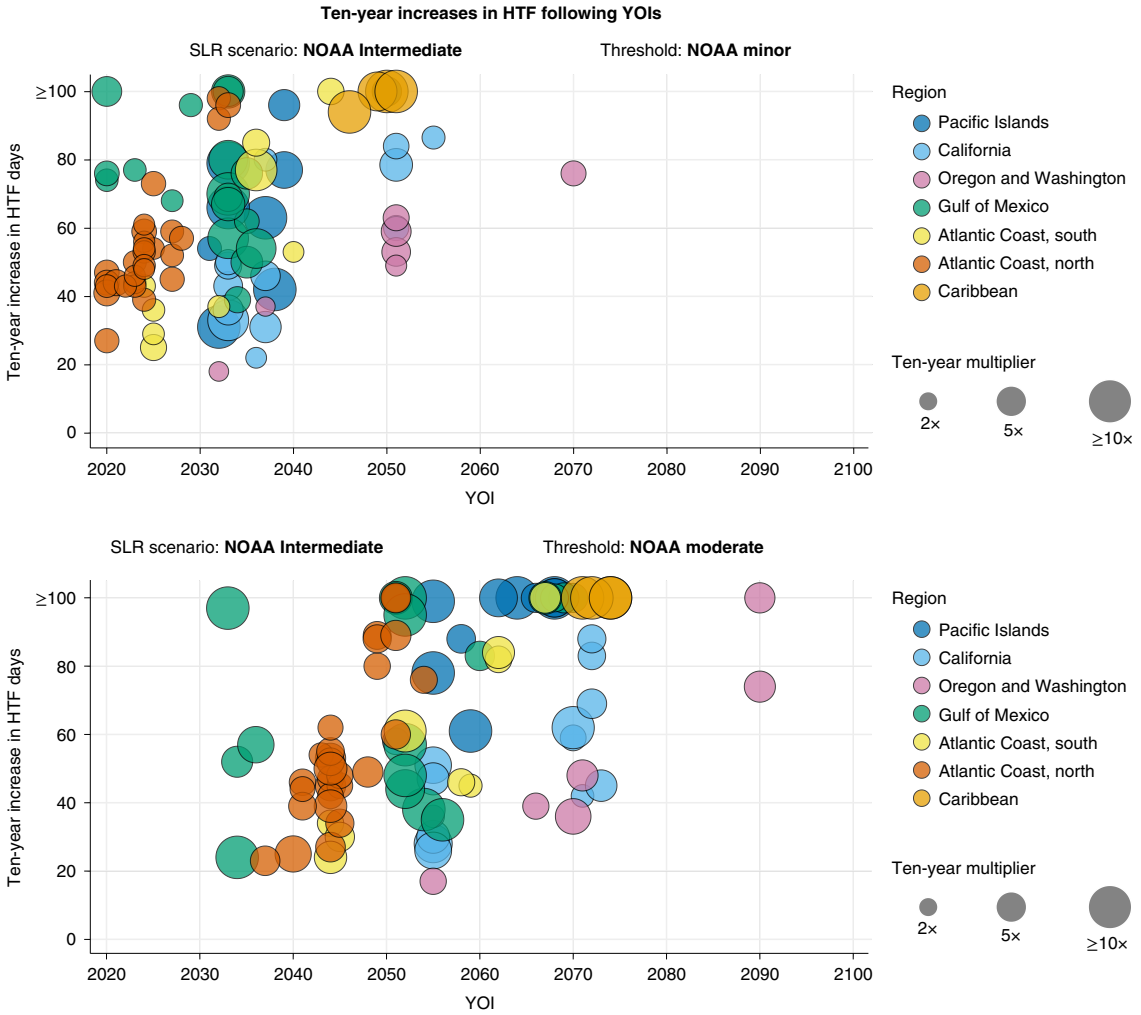

Fig. 3 | YOIs for the NOAA Intermediate SLR scenario. The upper and lower panels correspond to the NOAA minor and moderate flooding thresholds, respectively. The position along the horizontal axis corresponds to the timing of the YOI. The vertical axis indicates projected ten-year increases in annual counts of HTF days following YOIs. The dot sizes correspond to ten-year multipliers following the YOIs. The colours denote geographic regions. See Extended Data Fig. 2 for an analogous figure assuming the NOAA Intermediate Low SLR scenario.

for moderate thresholds tend to occur during periods when SLR rates are higher. As a result, the ten-year multipliers for decades following YOIs are larger for the moderate flooding thresholds than for the minor thresholds. For the Intermediate SLR scenario, 79% of locations would experience at least a fourfold increase in the HTF frequency above the moderate threshold during a single decade (compared with 39% for the minor threshold), and 35% would experience a sixfold increase during a single decade (compared with 20% for the minor threshold).

Clustering of HTF days

The 90th percentile of the ensemble spread for annual projections (Fig. 1) is expected to be exceeded about once per decade on average. Thus, year-to-year sea-level variability unrelated to secular SLR will lead to occasional but inevitable extreme years when many HTF days cluster together[19]. The 4.4-year modulation of tidal amplitude[32] can also contribute to extreme years, apparent in the HTF projection for La Jolla (Fig. 1) and other locations, especially the Pacific Coast and Southeast-Atlantic Bight (not shown). Clustering occurs at subannual timescales as well, and there are typically one or two seasons at any location for which the number of HTF days increases more rapidly due to annual and semiannual cycles in mean sea level and tidal amplitude (Extended Data Fig. 3). In Honolulu, for example, the most likely (50th percentile) annual count of HTF days in 2047 is 63 (Fig. 1). However, splitting the analysis into monthly counts reveals that 30 of those events are expected to occur over a span of three months (October–December, Extended Data Fig. 3). The expected temporal density of HTF days during this season (ten days per month) is thus approximately double that expected from considering the annual count alone (about five days per month). Similar differences in the seasonal density of HTF days are expected for the other three locations. Note that the seasonal timing of peaks in semiannual modulations of tidal amplitude (and hence HTF frequency) vary year to year and are linked to the 4.4-year modulations mentioned above[32].

The seasonal clustering of events can be further compounded by monthly to seasonal sea-level anomalies associated with modes of internal climate variability (for example, El Niño) or other atmosphere–ocean processes. If, for example, a large monthly mean sea-level anomaly occurs during peak HTF season, the two factors produce elevated numbers of HTF days during a brief period that far exceeds the expected annual density of events[33]. To demonstrate the impact of clustering, we calculate the average number of HTF days per month in five-year periods for the four locations

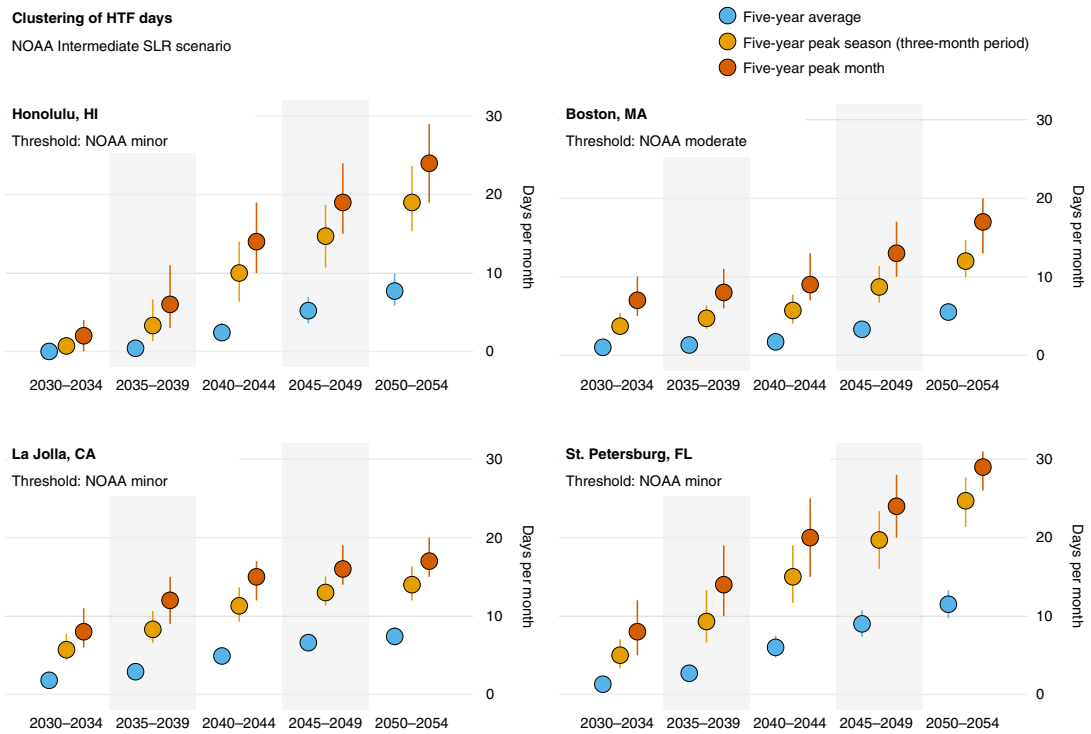

Fig. 4 | Extreme months and seasons. Projections of HTF days in five-year periods for the four US stations in Fig. 1 under the NOAA Intermediate SLR scenario, including the average number of HTF days per month in each five-year period (blue), the average number of HTF days per month during the five-year peak season (light orange) and the number of HTF days in the five-year peak month (dark orange). The circles represent the 50th percentile from the ensemble. The vertical lines show the 10th–90th percentiles of the ensemble range.

(Fig. 4). Using the ensemble projections, we also estimate the counts of HTF days during the most extreme season (that is, consecutive three-month period) and most extreme individual month over each five-year span (Fig. 4). For example, the 2040–2044 pentad in Honolulu is projected to experience ~2.5 minor HTF days per month on average (or about 150 minor HTF days over the entire five-year span). However, projected counts of minor HTF days during the most extreme season and month during this five-year span are 6–14 and 10–19 HTF days per month, respectively. Similar clustering is expected for St. Petersburg, while the effect is smaller for Boston and La Jolla. In general, using the expected number of HTF days per year (or pentad or decade) for decision-making will greatly underestimate the cumulative impact during brief periods experiencing extreme numbers of HTF days.

Another consequence of clustering is that any given HTF frequency will occur during brief periods long before it becomes expected on an annual basis. For example, consider the case for which minor flooding occurs on a majority of days during a given period. For most locations under the Intermediate scenario, this frequency of minor HTF will not occur on an annual basis until the second half of the twenty-first century[10]. Projections of minor HTF confirm this timeline for annual periods (Fig. 5, top row). However, if the focus shifts to monthly periods and includes the impact of clustering, we find that the timeline for experiencing flooding on a majority of days during a given period shifts towards the present (Fig. 5, bottom three rows). To estimate the importance of this effect, we calculated the probability that each location will experience minor flooding on a majority of days during a single month at least two decades before the year when minor flooding becomes expected on a majority of days annually. The probabilities were calculated by determining the fraction of projection ensemble members for each location that met this criterion. For the Intermediate scenario, this probability exceeds 50% (that is, it is more likely than not) at 42% of the locations analysed. The percentage increases to 81% of stations for lead times of 15 or more years. By incorporating the combined effects of month-to-month variations in mean sea level and tidal amplitude, our results suggest that planning horizons based on the emergence time[34] of a particular HTF frequency may need to be adjusted by decades towards the present to account for the clustering of HTF days during extreme months.

Discussion

Multiple strategies have been developed to identify key impact thresholds in terms of either HTF frequency[5] or the cumulative economic impact of frequent HTF events[3]. The YOI calculation here complements existing metrics by focusing on the pace of change and identifying the onset (rather than the endpoint) of rapid increases from few to many expected HTF events per year. The application of adaptation pathways requires updating policy and management strategies when predetermined environmental triggers or decision points occur[12–14]. Site-specific YOIs are candidates for such decision points, and the methodology underpinning the calculation provides important environmental context for stakeholders and decision-makers. In particular, nodal cycle modulations of tidal amplitude will suppress SLR-induced increases in HTF during certain periods and may delay the onset of environmental adaptation triggers. Such delays could produce complacency and inaction through false confidence in benign pathways. The effect of the nodal cycle is implicit in the YOI calculation, which will allow decision-makers and stakeholders to communicate that periods of little perceptible change are expected in many locations—only to be followed by periods of exponential HTF increase.

In general, if SLR approaches or exceeds the NOAA Intermediate scenario in the coming decades, the United States should expect the

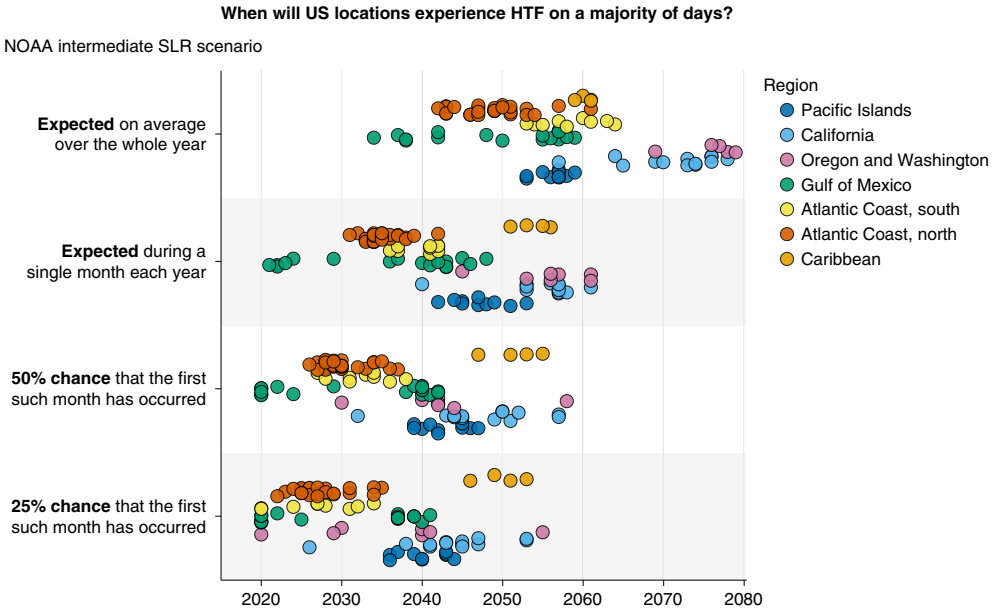

Fig. 5 | Years for which US coastal locations will experience HTF on a majority of days during annual and monthly windows. The calculations assume the NOAA Intermediate SLR scenario. Years for which HTF is expected to occur on a majority of days on average during annual and monthly periods (top two rows) are compared with years for which flooding will first occur on a majority of days during a single month (bottom two rows). The dot colours denote station regions. The vertical position of each dot within the rows is an arbitrary vertical offset to allow visual distinction between regions and individual locations. See Extended Data Fig. 4 for an analogous figure assuming the NOAA Intermediate Low SLR scenario.

onset of a rapid increase in HTF frequency during the mid-2030s corresponding to the combined effects of ongoing SLR and increasing tidal amplitude associated with nodal cycle modulations. The increase would be concentrated along the continental Pacific, Pacific Island and Gulf of Mexico coastlines, which are more vulnerable to SLR due to relatively narrow sea-level distributions[35], infrequent historical exposure to high storm surge[14] or both. Thus, under the NOAA Intermediate SLR scenario, the mid-2030s marks the onset of an expected transition in HTF from a regional issue to a national issue with a majority of US coastlines being affected. An important caveat to this result is that the YOIs represent the most likely inflection point, and decadal fluctuations in local mean sea levels may affect its timing.

The cumulative nature of impacts associated with minor HTF[1–3] suggests the need to account for severe seasons or months during which many HTF days cluster together in time. Just as engineers and coastal planners are accustomed to planning for rare, large-amplitude extreme events, adaptation and mitigation strategies focused on HTF should account for brief periods experiencing an extreme number of HTF days. The logic for basing decision-making on severe periods of HTF is the same as for basing design decisions on long (10-year or 100-year) return intervals rather than annual maxima, where the former has a planning horizon far in advance of the latter. Knowledge of the tendency for HTF days to cluster in time can aid the interpretation of HTF projections with coarse (annual and longer) temporal resolutions. On the basis of an aggregate analysis of clustering calculations across all US locations (not shown), we suggest the following rules of thumb for interpreting such projections. For a five-year period expected to experience a total of 100 HTF days, the six most severe months will experience 7–10 HTF days per month on average, while the remaining months will experience fewer than 1 HTF day per month on average. For 200 total HTF days over a five-year period, the six most severe months will experience 10–17 HTF days per month on average, while the remaining months will experience fewer than 2.5 HTF days per month on average. Importantly, this tendency for HTF days to cluster in time underscores the need for monthly-to-seasonal forecasting of sea-level anomalies to provide advance warning of periods likely to experience extreme numbers of events[36,37]. It is also possible that event clustering will be influenced by non-stationarity in the statistics of extreme non-tidal sea-level anomalies[38], which have not been considered here.

Finally, we reiterate that our analysis focused on existing and widely used NOAA SLR scenarios and derived HTF thresholds. The results are therefore unique to the specific combinations of location, SLR scenario and flooding threshold. As SLR continues and communities adapt, locally relevant flooding thresholds will evolve, and periodic reassessments will be required. Nevertheless, the concepts presented here are broadly applicable in identifying planning horizons and developing adaptation pathways for managing ongoing and future impacts of HTF. There is a need for nuanced understanding of projected increases in HTF frequency beyond quantifying, for example, bulk changes from one decade to the next. It is important to communicate to decision-makers that changes in HTF frequency will not be incremental in the coming decades but will include acute inflections in the rate of increase punctuated by extreme months and seasons during which many events will cluster together in time. These results form the basis of ongoing work to communicate projected increases in HTF to US decision-makers[39].

Online content

Any methods, additional references, Nature Research reporting summaries, source data, extended data, supplementary information, acknowledgements, peer review information; details of author contributions and competing interests; and statements of data and code availability are available at https://doi.org/10.1038/s41558-021-01077-8.

Received: 9 November 2020; Accepted: 4 May 2021;
Published online: 21 June 2021

References

1. Moftakhari, H. R., AghaKouchak, A., Sanders, B. F. & Matthew, R. A. Cumulative hazard: the case of nuisance flooding. *Earth's Future* **5**, 214–223 (2017).
2. Moftakhari, H. R., AghaKouchak, A., Sanders, B. F., Allaire, M. & Matthew, R. A. What is nuisance flooding? Defining and monitoring an emerging challenge. *Water Resour. Res.* **54**, 4218–4227 (2018).
3. Ghanbari, M., Arabi, M. & Obeysekera, J. Chronic and acute coastal flood risks to assets and communities in southeast Florida. *J. Water Resour. Plan. Manage.* **146**, 04020049 (2020).
4. Hino, M., Belanger, S. T., Field, C. B., Davies, A. R. & Mach, K. J. High-tide flooding disrupts local economic activity. *Sci. Adv.* https://doi.org/10.1126/sciadv.aau2736 (2019).
5. Sweet, W. V. & Park, J. From the extreme to the mean: acceleration and tipping points of coastal inundation from sea level rise. *Earth's Future* **2**, 579–600 (2014).
6. Wdowinski, S., Bray, R., Kirtman, B. P. & Wu, Z. Increasing flooding hazard in coastal communities due to rising sea level: case study of Miami Beach, Florida. *Ocean Coast. Manage.* **126**, 1–8 (2016).
7. Ray, R. D. & Foster, G. Future nuisance flooding at Boston caused by astronomical tides alone. *Earth's Future* **4**, 578–587 (2016).
8. Burgos, A. G., Hamlington, B. D., Thompson, P. R. & Ray, R. D. Future nuisance flooding in Norfolk, VA from astronomical tides and annual to decadal internal climate variability. *Geophys. Res. Lett.* **45**, 12432–12439 (2018).
9. Dahl, K. A., Fitzpatrick, M. F. & Spanger-Siegfried, E. Sea level rise drives increased tidal flooding frequency at tide gauges along the U.S. East and Gulf Coasts: projections for 2030 and 2045. *PLoS ONE* **12**, e0170949 (2017).
10. Sweet, W. V., Dusek, G., Obeysekera, J. & Marra, J. J. *Patterns and Projections of High Tide Flooding along the U.S. Coastline Using a Common Impact Threshold* NOAA Technical Report NOS CO-OPS 086 (US Department of Commerce, National Oceanic and Atmospheric Administration, National Ocean Service Center for Operational Oceanographic Products and Services, 2018).
11. Sweet, W. et al. *2019 State of U.S. High Tide Flooding with a 2020 Outlook* NOAA Technical Report NOS CO-OPS 092 2019 (US Department of Commerce, National Oceanic and Atmospheric Administration, National Ocean Service Center for Operational Oceanographic Products and Services, 2020).
12. Kwadijk, J. C. J. et al. Using adaptation tipping points to prepare for climate change and sea level rise: a case study in the Netherlands. *WIREs Clim. Change* **1**, 729–740 (2010).
13. Barnett, J. et al. A local coastal adaptation pathway. *Nat. Clim. Change* **4**, 1103–1108 (2014).
14. Stephens, S. A., Bell, R. G. & Lawrence, J. Developing signals to trigger adaptation to sea-level rise. *Environ. Res. Lett.* **13**, 104004 (2018).
15. Pugh, D. & Woodworth, P. *Sea-Level Science* (Cambridge Univ. Press, 2014).
16. Haigh, I. D., Eliot, M. & Pattiaratchi, C. Global influences of the 18.61 year nodal cycle and 8.85 year cycle of lunar perigee on high tidal levels. *J. Geophys. Res. Oceans* **116**, C06025 (2011).
17. Li, S. et al. Evolving tides aggravate nuisance flooding along the U.S. coastline. *Sci. Adv.* **7**, eabe2412 (2021).
18. Taherkhani, M. et al. Sea-level rise exponentially increases coastal flood frequency. *Sci. Rep.* **10**, 6466 (2020).
19. Thompson, P. R., Widlansky, M. J., Merrifield, M. A., Becker, J. M. & Marra, J. J. A statistical model for frequency of coastal flooding in Honolulu, Hawaii, during the 21st century. *J. Geophys. Res. Oceans* **124**, 2787–2802 (2019).
20. Tebaldi, C., Strauss, B. H. & Zervas, C. E. Modelling sea level rise impacts on storm surges along US coasts. *Environ. Res. Lett.* **7**, 014032 (2012).
21. Marcos, M., Calafat, F. M., Berihuete, Á. & Dangendorf, S. Long-term variations in global sea level extremes. *J. Geophys. Res. Oceans* **120**, 8115–8134 (2015).
22. Buchanan, M. K., Oppenheimer, M. & Kopp, R. E. Amplification of flood frequencies with local sea level rise and emerging flood regimes. *Environ. Res. Lett.* **12**, 064009 (2017).
23. Wahl, T. et al. Understanding extreme sea levels for broad-scale coastal impact and adaptation analysis. *Nat. Commun.* **8**, 16075 (2017).
24. Sweet, W. V. et al. *Global and Regional Sea Level Rise Scenarios for the United States* NOAA Technical Report NOS CO-OPS 083 (US Department of Commerce, National Oceanic and Atmospheric Administration, National Ocean Service Center for Operational Oceanographic Products and Services, 2017); https://doi.org/10.7289/V5/TR-NOS-COOPS-083
25. Hamlington, B. D., Leben, R. R., Strassburg, M. W., Nerem, R. S. & Kim, K. Contribution of the Pacific Decadal Oscillation to global mean sea level trends. *Geophys. Res. Lett.* **40**, 5171–5175 (2013).
26. Nerem, R. S. et al. Climate-change-driven accelerated sea-level rise detected in the altimeter era. *Proc. Natl Acad. Sci. USA* **115**, 2022–2025 (2018).
27. Han, W. et al. Impacts of basin-scale climate modes on coastal sea level: a review. *Surv. Geophys.* **40**, 1493–1541 (2019).
28. Kopp, R. E. et al. Probabilistic 21st and 22nd century sea-level projections at a global network of tide-gauge sites. *Earth's Future* **2**, 383–406 (2014).
29. IPCC *Climate Change 2013: The Physical Science Basis* (eds Stocker, T. F. et al.) (Cambridge Univ. Press, 2013).
30. Peng, D., Hill, E. M., Meltzner, A. J. & Switzer, A. D. Tide gauge records show that the 18.61-year nodal tidal cycle can change high water levels by up to 30 cm. *J. Geophys. Res. Oceans* **124**, 736–749 (2019).
31. Peltier, W. R. & Tushingham, A. M. Influence of glacial isostatic adjustment on tide gauge measurements of secular sea level change. *J. Geophys. Res. Solid Earth* **96**, 6779–6796 (1991).
32. Ray, R. D. & Merrifield, M. A. The semiannual and 4.4-year modulations of extreme high tides. *J. Geophys. Res. Oceans* **124**, 5907–5922 (2019).
33. Yoon, H., Widlansky, M. J. & Thompson, P. R. Nu'a Kai: flooding in Hawaii caused by a 'stack' of oceanographic processes [*in 'State of the Climate in 2017'*]. *Bull. Am. Meteorol. Soc.* **99**, S88–S89 (2018).
34. Hague, B. S., McGregor, S., Murphy, B. F., Reef, R. & Jones, D. A. Sea level rise driving increasingly predictable coastal inundation in Sydney, Australia. *Earth's Future* **8**, e2020EF001607 (2020).
35. Rueda, A. et al. A global classification of coastal flood hazard climates associated with large-scale oceanographic forcing. *Sci. Rep.* **7**, 5038 (2017).
36. Widlansky, M. J. et al. Multimodel ensemble sea level forecasts for tropical Pacific islands. *J. Appl. Meteorol. Climatol.* **56**, 849–862 (2017).
37. Jacox, M. G. et al. Seasonal-to-interannual prediction of North American coastal marine ecosystems: forecast methods, mechanisms of predictability, and priority developments. *Prog. Oceanogr.* **183**, 102307 (2020).
38. Widlansky, M. J., Long, X. & Schloesser, F. Increase in sea level variability with ocean warming associated with the nonlinear thermal expansion of seawater. *Commun. Earth Environ.* **1**, 9 (2020).
39. Thompson, P. R. *Flooding Days Projection Tool.* https://sealevel.nasa.gov/flooding-days-projection/ (2019).

Methods

Projections of HTF days. The projection framework is based on the idea that the number of observed hourly flooding threshold exceedances in a month—including the combined effect of tides, surge and other high-frequency contributions—is statistically related to monthly mean sea level and the amplitude of the highest tides during the month. For higher monthly mean sea level or tidal amplitude, there is a tendency to experience a greater number of flooding threshold exceedances, because the baseline sea level is higher. A higher baseline means that smaller-amplitude, more common surges can raise the total water level above the threshold.

An overview of the projection methodology is as follows:

1. Find a statistical relationship that maps monthly mean sea level, tidal amplitude and threshold height onto observed monthly counts of threshold exceedances in hourly tide-gauge data. The hourly tide-gauge data includes high-frequency surge and so on.
2. Generate ensemble projections of monthly mean sea level and tidal amplitude for the twenty-first century.
3. Map the ensemble projections of mean sea level and tidal amplitude from step 2 onto future counts of threshold exceedances using step 1. The resultant ensemble projections of threshold exceedances (that is, HTF) represent a range of possibilities for the number of exceedances a tide gauge would be expected to observe during a given future month.

The details of these steps are provided in the subsequent sections.

Relating tidal range, mean sea level and counts of HTF days. The methodology employed here builds on an approach previously developed for projecting the frequency of HTF in Honolulu, Hawai'i[19]. The fundamental assertion of this approach is that the probability distribution governing the number of HTF days at a given location during a single month is closely related to a single parameter, Δ_{99}:

$$\Delta_{99} \equiv (\zeta_{99} + \overline{\eta}) - H, \tag{1}$$

where ζ_{99} is the 99th percentile of predicted astronomical hourly tidal heights relative to current tidal datums, $\overline{\eta}$ is the monthly mean of the non-tidal sea level variability and H is the height of the flooding threshold of interest. Previous work focused on annual periods; here we calculate monthly values of ζ_{99} and $\overline{\eta}$ to produce monthly values of Δ_{99}. The term in parentheses, $\zeta_{99} + \overline{\eta}$, provides a general measure of the height of high tides during a given month. The specific role of ζ_{99} is to capture variability in high-tide levels due to seasonal-to-decadal modulations of tidal range. Note that the results herein are not sensitive to the particular percentile used. The specific role of $\overline{\eta}$ is to capture variability in high-tide levels due to changes in the mean level about which the tides oscillate. By subtracting the threshold height, H, from this sum, we can interpret variability in Δ_{99} as a measure of whether high tides are generally higher (more positive Δ_{99}) or lower (more negative Δ_{99}) than the threshold for a given month. The presence of stochastic, submonthly water level variability prevents relating Δ_{99} to a specific monthly count of threshold exceedances. Instead, we state that the Δ_{99} parameter is related to the probability mass distribution (PMD) governing the number of days during a month for which the maximum hourly water level exceeds the threshold. In other words, we cannot precisely predict the observed number of threshold exceedances on the basis of monthly quantities, because we do not know the exact number and magnitude of high-frequency anomalies that will occur in the future. We can, however, predict the likelihood of any given number of threshold exceedances on the basis of the observed historical relationships between mean sea level, tidal amplitude and threshold exceedances.

To demonstrate the relationship between Δ_{99} and monthly counts of HTF days, we first calculate observed values of ζ_{99} and $\overline{\eta}$ using hourly tide-gauge observations. We then tally the number of daily maximum water levels that exceed a range of thresholds in each month (that is, monthly counts of HTF days) and record the Δ_{99} value corresponding to each monthly count. Scatter plots of January HTF day counts versus January values of Δ_{99} for Honolulu and Boston, respectively, give insight into the functional form relating the two quantities (Extended Data Fig. 5). As expected, increasing Δ_{99} (that is, high tides rising relative to the threshold) corresponds to greater numbers of HTF days in each month. Note that the domain of Δ_{99} values is much narrower for Honolulu than for Boston, reflecting a much narrower distribution of daily maximum water levels for the former than for the latter. It is also important to note that the relationship between Δ_{99} and HTF days is nonlinear, and a unit change in Δ_{99} leads to varying increases in HTF days depending on the value of Δ_{99}.

To capture the probabilistic relationship between Δ_{99} and the monthly counts of HTF days, we model the PMD for monthly counts of HTF days as a beta-binomial distribution[40]. The beta-binomial distribution describes the probability of a discrete number of successes over N binary trials, where the probability that any single trial is a success is itself a continuous beta-distributed random variable, $p \in [0, 1]$. In this case, each of the N days in a month is a 'trial', and each time the daily maximum water level exceeds the threshold of interest is a 'success'. The beta distribution governing p can be described by its mean, μ, and variance, σ^2. Because p is beta-distributed, the beta-binomial distribution offers a general representation of binomially distributed counts that can take a variety of shapes. The flexibility of the beta-binomial distribution is useful, because the shape of the PMD for the monthly counts changes drastically depending on the value of Δ_{99}. For example, when Δ_{99} takes a large negative value (that is, when the highest tides of the month are well below the threshold), we expect a highly asymmetric, one-sided PMD with a high probability of zero exceedances and a low probability of many exceedances. As Δ_{99} increases to an expected (or mean) count of 10–20 days per month, the distribution of counts about the mean becomes approximately symmetric. As Δ_{99} increases further, the distribution becomes asymmetric and one-sided again as the counts begin to saturate at the maximum number of days per month.

We use the beta-binomial distribution to formulate a hierarchical model describing the probabilistic relationships between the vector of observed monthly counts of HTF days ($\mathbf{Y}$) and the vector of observed Δ_{99} values ($\mathbf{x}$). The model is summarized

$$\begin{aligned} \mathbf{Y} \,|\mathbf{x},\ \boldsymbol{\Theta},\ \nu\ &\sim\ \text{BetaBinomial}(N, \boldsymbol{\mu}, \boldsymbol{\sigma}^2), \\ \boldsymbol{\mu}\ &=\ S(\mathbf{x}; \boldsymbol{\Theta}), \\ \boldsymbol{\sigma}^2\ &=\ \nu\boldsymbol{\mu}(1-\boldsymbol{\mu}), \end{aligned} \tag{2}$$

where $\boldsymbol{\mu}$ and $\boldsymbol{\sigma}^2$ are vectors of μ and σ^2 that determine the shape of the beta-binomial distribution at each value in $\mathbf{x}$. The elements in $\boldsymbol{\sigma}^2$ are related to the elements in $\boldsymbol{\mu}$ by a scalar parameter, $\nu \in (0, 1)$, and the third relation in equation (2), which can be derived from the analytical function describing the distribution. This leaves only μ to be defined explicitly as a function of x (that is, Δ_{99}), which is represented by a function S requiring parameters $\boldsymbol{\Theta}$.

Since μ describes the expectation value of the probability, p, that a single day experiences a maximum hourly water level above the threshold, and since daily maximum water levels at any given station tend to be approximately normally distributed, we base the function S on the normal cumulative distribution function:

$$\Phi(x) = \frac{1}{2}\left[1 + \text{erf}\left(\frac{x-\xi}{\omega\sqrt{2}}\right)\right], \tag{3}$$

where erf(·) is the Gauss error function, and ξ and ω are parameters representing the location and scale of the function, respectively. In practice, we found that using this function alone as in prior work[19] (that is, $S(x) = \Phi(x)$) did not perform optimally in many cases due to minor deviations from a purely normal distribution—namely, slight asymmetries in the distribution of daily maximum water levels. We improved the ability of the model to describe the observed counts by defining S as the sum of two normal cumulative distribution functions blended across a change point via a logistic function:

$$S(x; r, x_0, \xi_1, \omega_1, \xi_2, \omega_2) = L(x; -r, x_0)\Phi(x; \xi_1, \omega_1) + L(x; r, x_0)\Phi(x; \xi_2, \omega_2), \tag{4}$$

where $L(x)$ is a logistic function:

$$L(x) = \frac{1}{1 + e^{-r(x-x_0)}}, \tag{5}$$

with r determining the slope of the transition—note the sign change of r from the first to the second term in equation (4)—and x_0 determining the location of the change point. This blended version of S allows the shape of the function to be determined by ω_1 and ξ_1 for $x < x_0$ and ω_2 and ξ_2 for $x > x_0$ with a narrow, smooth transition band of length scale $1/r$ to avoid discontinuity. In practice, we fix the length scale to 10% of the Δ_{99} domain and treat the change point x_0 as a free parameter. The vector of parameters required for the S in the hierarchical model is then $\boldsymbol{\Theta} = \{x_0, \xi_1, \omega_1, \xi_2, \omega_2\}$.

We estimate distributions of the free parameters in equation (2)—that is, $\boldsymbol{\Theta}$ and ν—for each station individually using Bayesian inference implemented via a Markov chain Monte Carlo (MCMC) method. Bayesian inference via MCMC was implemented by building and evaluating the hierarchical model in PyMC3 (ref. [41]), an open-source probabilistic programming framework for Python. Uninformative uniform prior distributions were assumed for all model parameters. Posterior distributions for the parameters were conditioned on vectors of observed monthly counts ($\mathbf{Y}$) and Δ_{99} values ($\mathbf{x}$) such as those represented by the scatter plots in Extended Data Fig. 5. Given the posterior distributions for the free parameters, we can then input a monthly value for Δ_{99} as $\mathbf{x}$ into equation (2) and output a probability distribution for the monthly count of HTF days above a threshold. The posterior models for Honolulu and Boston demonstrate the ability of the method to capture the probabilistic relationships underlying the scatter plots (Extended Data Fig. 5). Thus, given a projection (or ensemble of projections) of Δ_{99} during the twenty-first century, we can produce probabilistic projections for monthly counts of HTF days above a threshold.

Twenty-first-century projections of Δ_{99}. Projecting future Δ_{99} values for each station and threshold during the twenty-first century requires projections of ζ_{99} and $\overline{\eta}$ in equation (1). The latter is composed of two components: (1) secular local mean sea level (LMSL) rise related to forced climate variability and vertical land motion, and

(2) stochastic monthly LMSL variability related to atmosphere–ocean dynamics and internal climate variability. This gives three components of Δ_{99} (ζ_{99} plus two components of $\overline{\eta}$), which we project independently as discussed below.

Secular LMSL rise projections. We use the NOAA local SLR scenarios[24] obtained from the NOAA Center for Operational Oceanographic Products and Services (CO-OPS, https://tidesandcurrents.noaa.gov/publications/techrpt083.csv). These are discrete projections with predetermined amounts of LMSL rise by 2100, which are designed to provide planning scenarios corresponding to various risk tolerances. The scenarios for each site include local factors such as glacial isostatic adjustment and regional patterns of sea level change due to the gravitational and rotational effects of melting glaciers and ice sheets. We focus on the Intermediate Low and Intermediate scenarios, which correspond to twenty-first-century global mean SLR of 0.5 m and 1.0 m, respectively. The NOAA scenarios are provided with decadal resolution, which we interpolate to monthly resolution via cubic spline.

Projecting monthly LMSL variability. Gaussian processes have been used previously to model parameters relating mean sea level variability and HTF[42]. We modelled non-secular monthly LMSL variability, $m(t)$, as the weighted sum of a zero-mean Gaussian process with unit variance G and normally distributed white noise with zero mean and unit variance Σ:

$$m(t) = aG + b\Sigma\,. \tag{6}$$

Serial correlation in G is determined by an exponentiated quadratic covariance function, K:

$$K(t,t') = \exp\left[\frac{(t-t')^2}{2l^2}\right], \tag{7}$$

where l is a timescale. The distributions of the free parameters, $\{a, b, l\}$, were determined from observed monthly mean tide-gauge observations for each station via Bayesian inference and MCMC using PyMC3 (ref. [41]). Given the variance in the observed non-secular monthly mean sea level time series, σ_m^2, the parameters a and b were chosen from a multivariate beta (or Dirichlet) prior to ensure that $a^2 + b^2 = \sigma_m^2$ and for any given draw from the posterior. The parameter l was given an uninformative gamma-distributed prior. We generated an ensemble of 10^4 posterior samples of $m(t)$ spanning the twenty-first century for each US tide-gauge station.

99th percentile of astronomical tides. Tides are often treated as if they are unchanging in HTF assessments, and tide predictions are often performed and interpreted as if they are free from uncertainty. These are not good assumptions in many locations[17] due to correlations of tidal amplitude with mean sea level variability[43] and changes in the geometry of harbours and estuaries[44]. Here, we generate an ensemble of tide predictions for each location that accounts for portions of the non-stationarity in future tidal amplitudes. In particular, we include the observed relationship between mean sea level variability and constituent amplitudes and phases, and we include an extrapolation of secular trends in tidal amplitude and phase that are unrelated to mean SLR. Our method does not represent a complete accounting of the uncertainty and sources of non-stationarity—and some assumptions have been made—but the result is preferable to not considering non-stationarity and uncertainty in the tides.

Ensemble projections of ζ_{99} were determined for each location individually in a multistep process:

1. Generate an initial estimate of tidal constituents from harmonic analysis of hourly tide-gauge data. For this initial step, tidal constituents were estimated from the complete record using an implementation of UTide[45] for Python. Note that the development of UTide for Python is ongoing, but comparisons of UTide predictions to NOAA tide predictions suggest that results from the former are robust.
2. Distinguish between minor and major constituents with signal-to-noise ratios less than two and greater than two, respectively.
3. Subtract predictions of minor constituents over the observed period and perform harmonic fits on the remaining hourly variability using UTide[45] for the major constituents in each year of the record individually. Year-to-year variations in major-constituent amplitudes and phases reflect both astronomical (for example, nodal cycle) and non-astronomical (for example, correlation with mean sea level[43]) processes.
4. Model the variability in the phases and amplitudes of each constituent as a sum of Gaussian processes with periodic and linear kernels, plus a term proportional to detrended annual mean sea level variability and an additional white-noise term. The periodic kernels represent major tidal modulation periodicities (18.61, 9.305, 8.85 and 4.425 years)[16]. Linear trends in the constituent amplitudes and phases were modelled as two linear processes linked at a variable change point, which allows for an inflection in the secular trend of each constituent and ensures that extrapolated linear trends in the amplitude and phase of each constituent are representative of the most recent trend. The change point was required to be consistent for both amplitude and phase. The model parameters and the relative weight of each component were determined via Bayesian inference and MCMC using PyMC3 (ref. [41]).
5. Generate an ensemble projection of each constituent individually from the components of amplitude and phase variability in the previous step. When projecting tidal variability for the twenty-first century, we confine the relationship with mean sea level to be a relationship with steric (or density-related) changes in mean sea level. In general, the relationship between mean sea level and constituent amplitude can be related to water depth or stratification, but it is difficult to disentangle these effects in the absence of dedicated, local modelling studies[46]. The decision to confine the relationship to steric changes in mean sea level is thus a conservative choice to limit overestimating this effect. Only the steric component of the NOAA SLR scenario used in each case is added to the ensemble of monthly LMSL variability (described earlier in the Methods) to produce estimates of steric sea level variability in the twenty-first century.
6. Construct an ensemble of 10^4 hourly twenty-first-century tidal height predictions from the ensemble of annual projections for each major constituent and add a deterministic prediction of the minor constituents. The Gaussian process representations underlying each major constituent allow us to construct tidal predictions with hourly resolution that modulate smoothly from one annual window to the next. Note that in every case, our methodology for tide prediction produces a reduction in non-tidal residual variability over the observed period compared with the standard NOAA harmonic analysis.
7. From the ensemble of hourly tidal height predictions, generate an ensemble of 10^4 projections of ζ_{99}.

Ensemble projections of HTF days. To produce ensemble twenty-first-century projections of HTF days above a given threshold, we performed the following procedure for each combination of station, SLR scenario and threshold:

1. Generate 10^4 projections of Δ_{99} by adding the ensemble of $\overline{\eta}$ projections (SLR scenario plus monthly variability) to the ensemble of ζ_{99} and subtracting the threshold height, H.
2. For each value in the ensemble of Δ_{99} projections, make a draw from the posterior of the model in equation (2).
3. Generate a random positive integer representing a monthly count of HTF days from the beta-binomial distribution described by each combination of Δ_{99} value and posterior draw.

The result is an ensemble of 10^4 twenty-first-century projections of HTF days per month for each combination of station, SLR scenario and threshold. We can then leverage these ensembles of monthly counts to generate likely ranges and assess the relationship of extreme months and seasons to counts over longer periods of years to decades. Note that the spread in each ensemble grows with SLR due to the nature of counting exceedances above a threshold (for example, the 10th–90th percentile ranges in Fig. 1). For example, when a threshold is rarely exceeded, most years will experience zero HTF days, and the range of possible annual counts is narrow (for example, zero to five HTF days per year). With SLR, exceedances become more common, and the range of possible annual counts grows.

Determination of YOIs. YOIs were identified using the 50th-percentile curve from the ensemble of annual HTF projections (see below) for each combination of location, scenario and threshold. Two characteristics of the 50th-percentile curve were used. The first is the difference in the change in HTF frequency between two adjacent ten-year periods, which is analogous to the second derivative of the 50th-percentile curve and is largest when the slope of the projection changes rapidly. There can be multiple acute inflections over a single projection, however, which motivated the use of a second quantity: the ten-year multiplier (or x-fold increase) over the second of the two adjacent ten-year periods. The ten-year multiplier is largest for inflections that represent a transition from few to many expected days of HTF per year. For example, a change from 10 to 50 HTF days per year over the second ten-year period has a multiplier of 5; a change from 50 to 100 has a multiplier of 2. In practice, we computed both quantities in sliding 21-year windows centred on each year in the HTF projection curves. We identified the YOI for each combination of location, scenario and threshold as the year with the highest average rank over both quantities.

Data availability

The tide-gauge sea-level data used in this analysis are publicly accessible and were obtained from the NOAA CO-OPS Data Retrieval API (https://api.tidesandcurrents.noaa.gov/api/prod/). The NOAA SLR scenarios are publicly available and were obtained from the NOAA CO-COPS website (https://tidesandcurrents.noaa.gov/publications/techrpt083.csv).

Code availability

All code generated for the data analysis and figure creation is archived in a public repository[47] under the GNU Affero General Public License v.3.0. The repository includes the Python environment, which provides the versions of all third-party libraries and packages used in this work.

References

40. Skellam, J. G. A probability distribution derived from the binomial distribution by regarding the probability of success as variable between the sets of trials. *J. R. Stat. Soc. B* **10**, 257–261 (1948).
41. Salvatier, J., Wiecki, T. V. & Fonnesbeck, C. Probabilistic programming in Python using PyMC3. *PeerJ Comput. Sci.* https://doi.org/10.7717/peerj-cs.55 (2016).
42. Vandenberg-Rodes, A. et al. Projecting nuisance flooding in a warming climate using generalized linear models and Gaussian processes. *J. Geophys. Res. Oceans* **121**, 8008–8020 (2016).
43. Devlin, A. T. et al. Coupling of sea level and tidal range changes, with implications for future water levels. *Sci. Rep.* **7**, 17021 (2017).
44. Familkhalili, R. & Talke, S. A. The effect of channel deepening on tides and storm surge: a case study of Wilmington, NC. *Geophys. Res. Lett.* **43**, 9138–9147 (2016).
45. Codiga, D. L. *Unified Tidal Analysis and Prediction Using the UTide Matlab Functions* Technical Report No. 2011-01 (Graduate School of Oceanography, University of Rhode Island, 2011); https://doi.org/10.13140/RG.2.1.3761.2008
46. Haigh, I. D. et al. The tides they are a-changin': a comprehensive review of past and future nonastronomical changes in tides, their driving mechanisms, and future implications. *Rev. Geophys.* **58**, e2018RG000636 (2020).
47. Thompson, P. R. Code repository for 'Rapid increases and extreme months in projections of United States high-tide flooding'. *Zenodo* https://doi.org/10.5281/zenodo.4723019 (2021).

Acknowledgements

P.R.T. acknowledges support from NASA grant no. 80NSSC17K0564 and NOAA grant no. NA16NMF4320058. M.J.W. acknowledges support from NOAA grant nos NA17OAR4310110 and NA19OAR4310292. B.D.H. acknowledges support from the NASA Sea-Level Change Team (N-SLCT, WBS no. 105393).

Author contributions

P.R.T. designed the approach, performed the analyses and drafted the paper. M.J.W., B.D.H. and M.A.M. made substantive revisions. All authors made substantive contributions to the interpretation and communication of the results.

Competing interests

The authors declare no competing interests.

Additional information

Extended data is available for this paper at https://doi.org/10.1038/s41558-021-01077-8.

Supplementary information The online version contains supplementary material available at https://doi.org/10.1038/s41558-021-01077-8.

Correspondence and requests for materials should be addressed to P.R.T.

Peer review information *Nature Climate Change* thanks Kristina Dahl, Ben Hague and Hamed Moftakhari for their contribution to the peer review of this work.

Reprints and permissions information is available at www.nature.com/reprints.

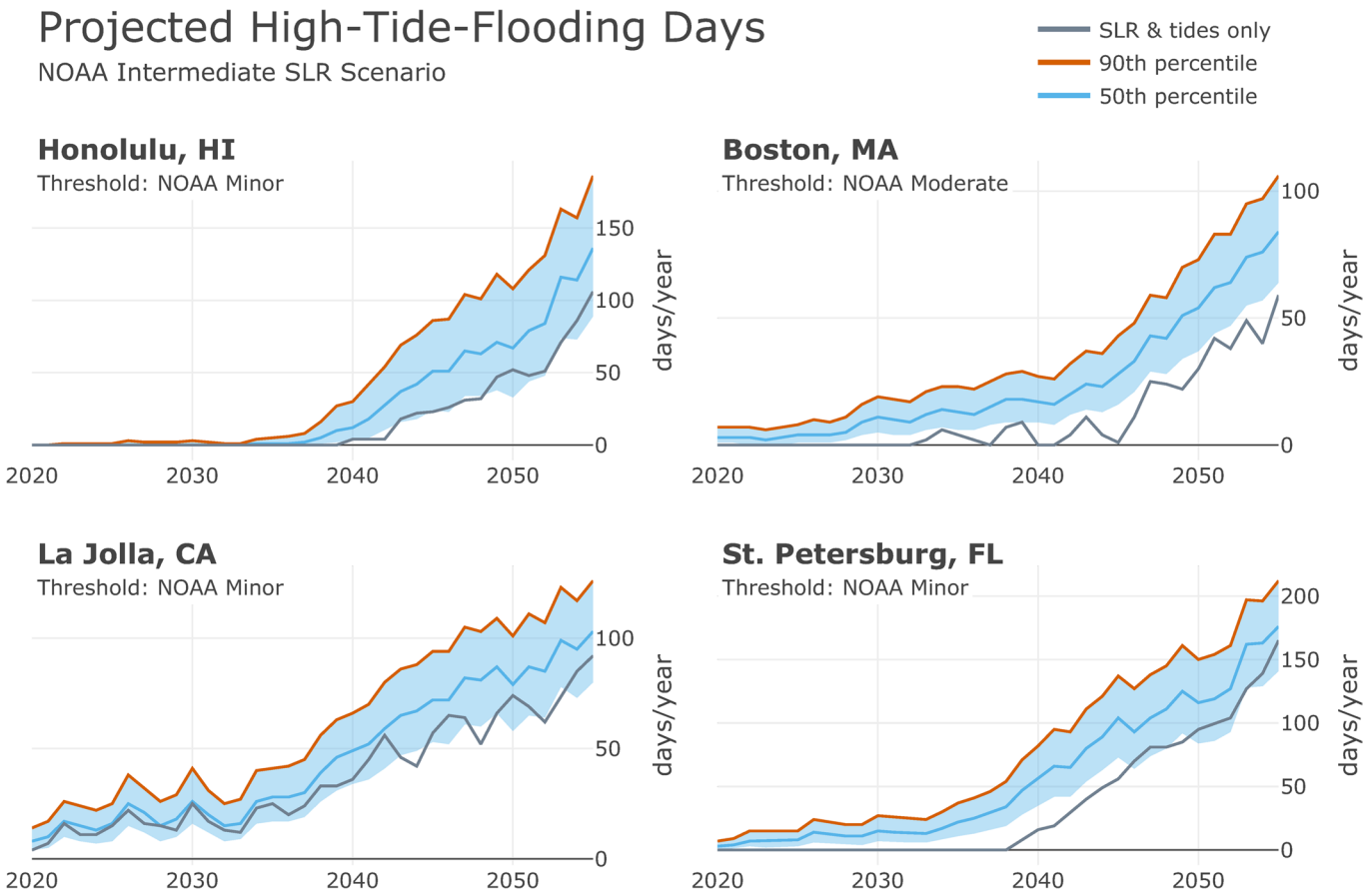

Extended Data Fig. 1 | Projections of annual counts of high-tide-flooding (HTF) days compared to expectations from SLR and tides alone. The four ensemble projections (blue) are identical to Fig. 1. The simple projection of HTF frequency based only on the SLR scenario and predictions of astronomical tides (gray) underestimates the frequency of HTF due to the exclusion of local mean sea level variability across a variety of time scales from high-frequency surge to decadal climate variability.

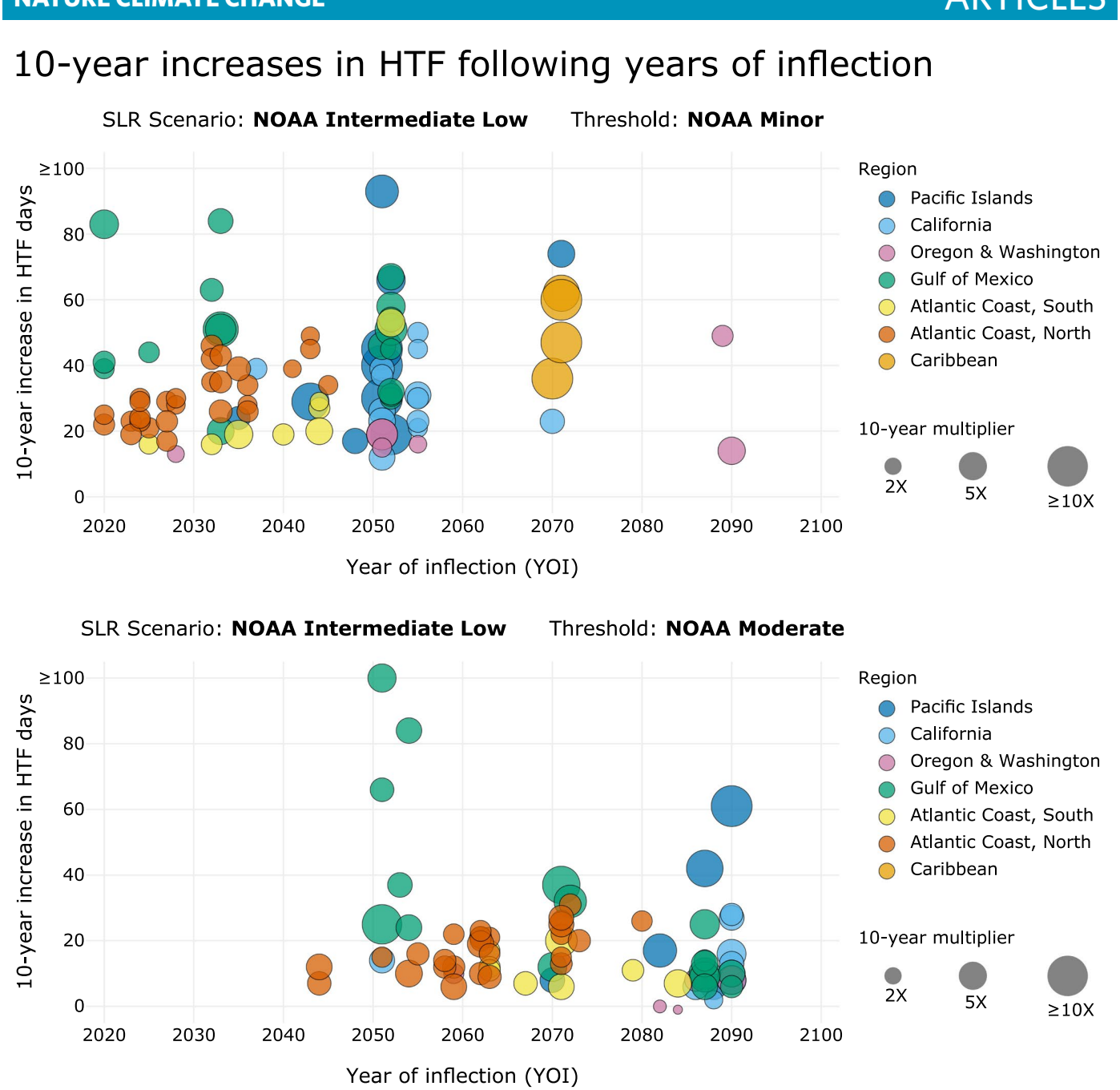

Extended Data Fig. 2 | Years of inflection (YOIs) for the NOAA Intermediate Low SLR scenario. The upper and lower panels correspond to the NOAA Minor and Moderate flooding thresholds, respectively. Position along the horizontal axis corresponds to the timing of the YOI. The vertical axis is projected ten-year increases in annual counts of HTF days following YOIs. Marker size corresponds to ten-year multipliers following the YOIs. Color denotes geographic region.

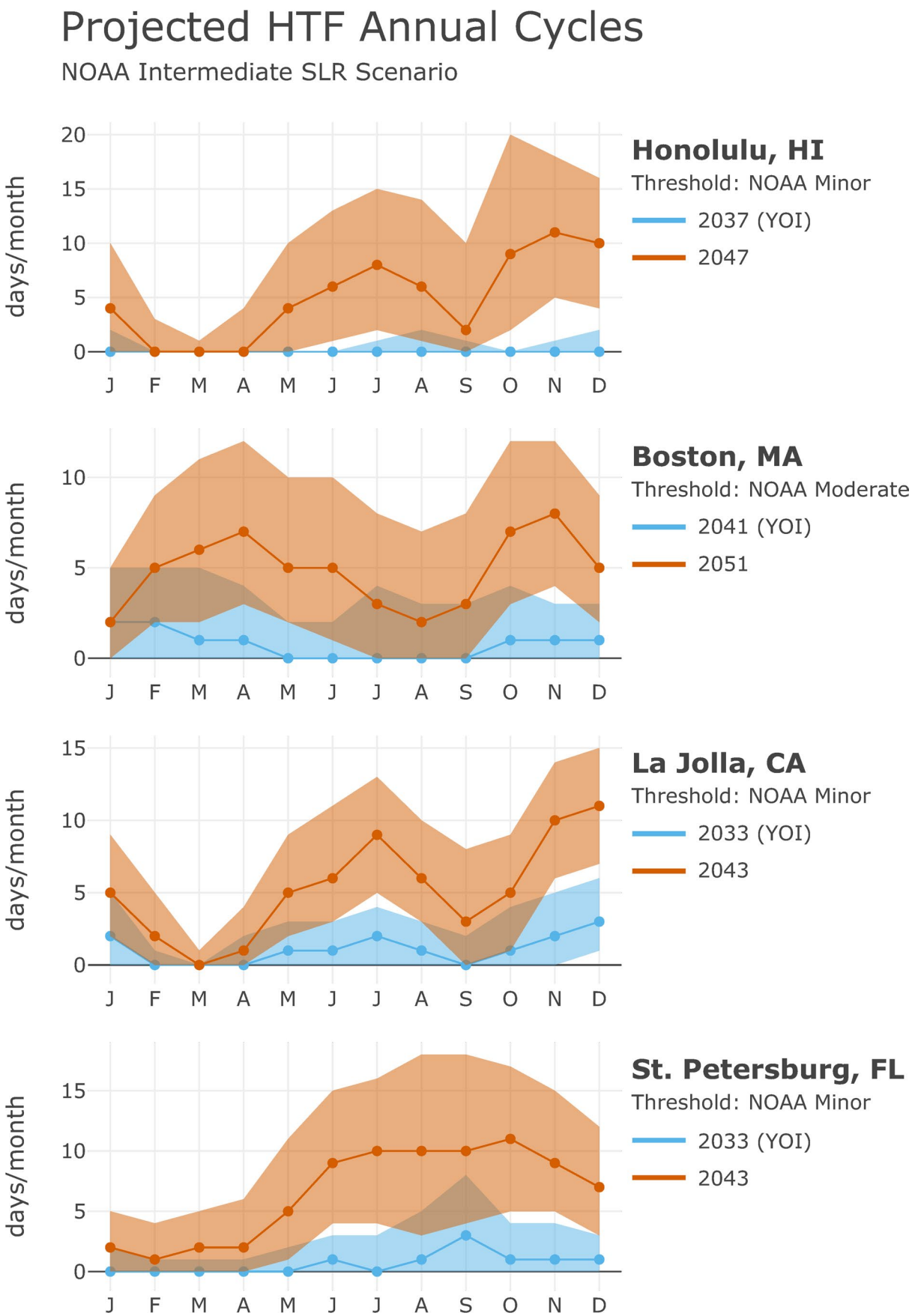

Extended Data Fig. 3 | Projected changes in the seasonal cycle of HTF frequency. Projections correspond to the YOI (blue) and 10 years later (orange) for the four US locations in Fig. 1 assuming the NOAA Intermediate SLR scenario. Shading shows the 10th–90th percentile intervals for each year and month.

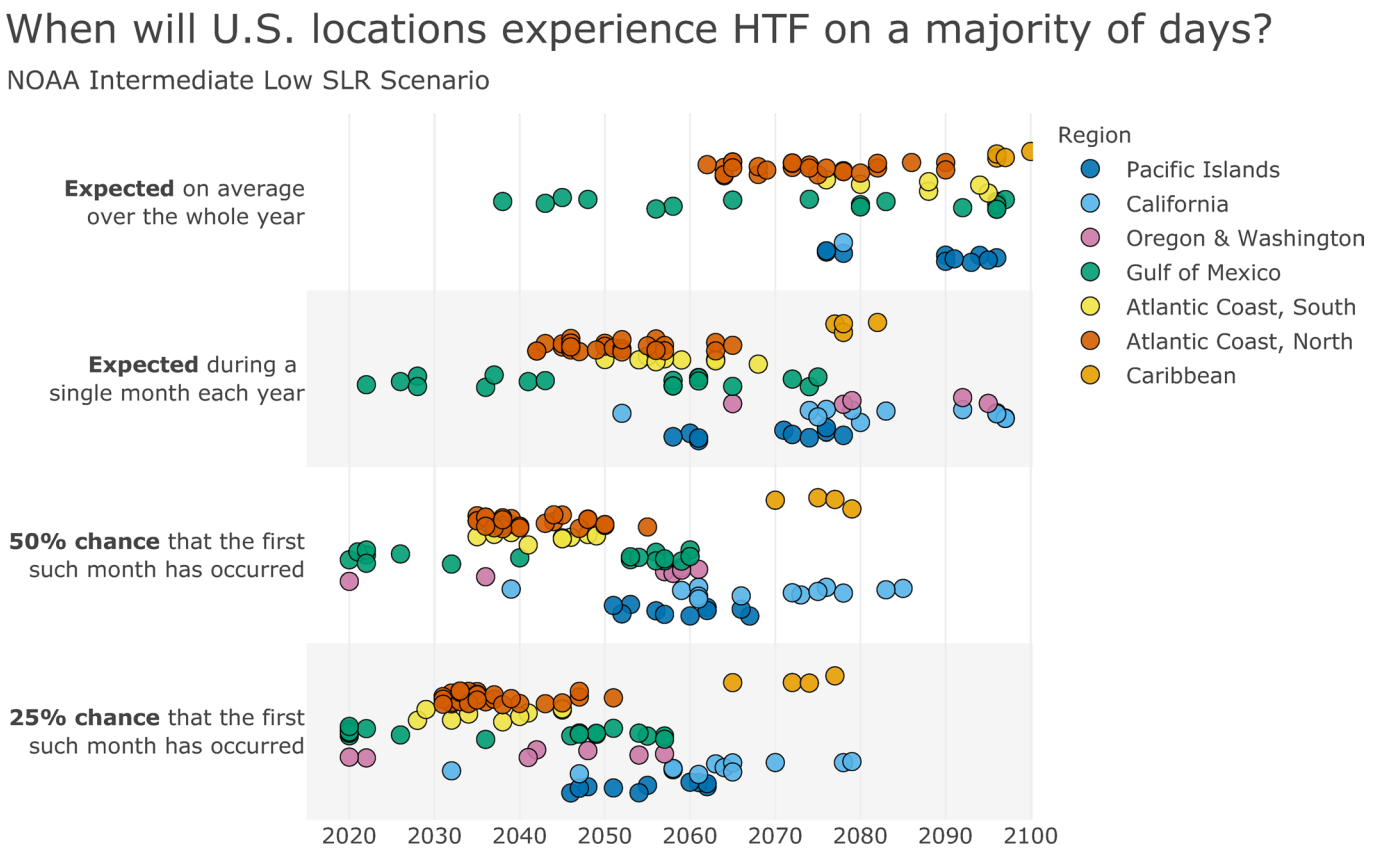

Extended Data Fig. 4 | Years for which U.S. coastal locations will experience HTF on a majority of days during annual and monthly windows. Calculations assume the Intermediate Low SLR scenario. Years for which HTF is expected to occur on a majority of days on average during annual and monthly periods (top two rows) are compared to years for which flooding will first occur on a majority of days during a single month (bottom two rows). Marker colors denote station region. The vertical position of each marker within the rows is an arbitrary vertical offset to allow visual distinction between regions and individual locations.

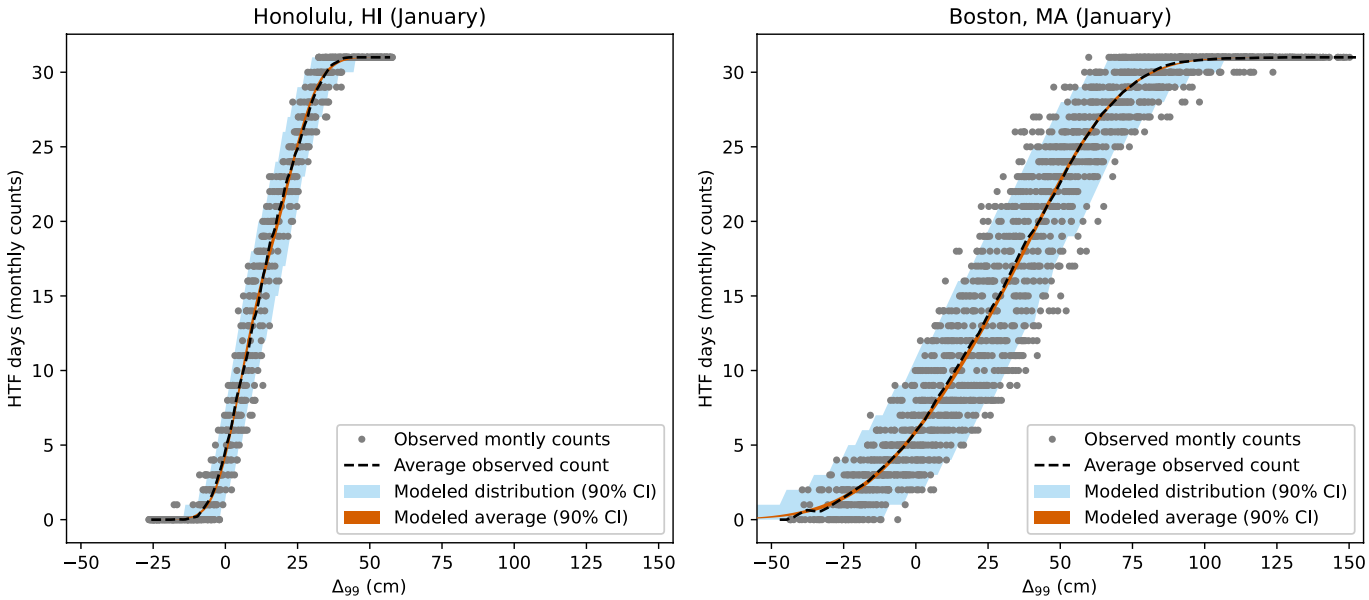

Extended Data Fig. 5 | Relationships between Δ_{99} and monthly counts of HTF days. Examples correspond to the observed (gray and black) and fitted (orange and red) relationships for the month of January in (a) Honolulu and (b) Boston.